

## A DIGITAL BACKGROUND CALIBRATION METHOD FOR TIME-INTERLEAVED ADCS BASED ON FREQUENCY SHIFTING TECHNIQUE

Yanze Zheng<sup>1)</sup>, Sitao Mei<sup>1)</sup>, Sicheng Sun<sup>1)</sup>, Yijiu Zhao<sup>1,2)</sup>

1) School of Automation Engineering, University of Electronic Science and Technology of China, Chengdu, China

2) Shenzhen Institute for Advanced Study, University of Electronic Science and Technology of China, Chengdu, China  
(✉ [yijiu@uestc.edu.cn](mailto:yijiu@uestc.edu.cn))

### Abstract

The presence of channel mismatches in time-interleaved analog-to-digital converters (TIADCs) seriously degrades the performance of the acquisition system. This paper presents a digital background calibration method to address gain and time skew mismatches. The spurious signals caused by gain and time skew mismatches can be represented by the frequency-shifted signals produced by modulating the TIADC output. To create frequency-shifted signals, the Hadamard transform is adopted. The advantage of the proposed calibration method is that it does not require any filters or complex signal processing structures, thus considerably decreasing the complexity of the calibration circuit. We have employed a four-channel TIADC system to validate the effectiveness of the proposed calibration technique. Moreover, it is demonstrated in a commercial 12.5 GSPS four-channel TIADC system, that this method improves the spurious free dynamic range of the system by 25 dB.

Keywords: TIADC system, mismatch calibration, frequency shifting, Hadamard transform.

### 1. Introduction

Analog-to-digital converters (ADCs) are critical components in many signal acquisition systems, such as 5G communication, radar, and instrumentation. Some high-speed applications often require ADCs with the sampling rate of several gigahertz (GHz) or even tens of GHz. Nevertheless, it is challenging to satisfy the requirement with a single ADC [1]. To address this issue, parallel sampling techniques have been proposed [2], and the *time-interleaved ADC* (TIADC) technique is one of the most prevalent solutions [3, 4]. It is a typical parallel system employing a bank of sub-ADCs with identical sampling rates but distinct sampling phases, which allows for a higher sampling rate than a single ADC. Ideally, each sub-ADC is completely identical, and all sampling phases are accurate. As a result, by rearranging the output of each sub-ADC, the performance of the TIADC would be comparable to that of a single ADC with a higher sampling rate. Unfortunately, such ideal conditions are virtually non-existent in a practical acquisition

system, and the performance of TIADCs suffers from mismatches among the sub-ADCs [5]. The presence of mismatches (offset, gain, and time skew) causes the output of the system to include spurious signals in addition to the desired signal components, which can seriously degrade the system performance [6]. Therefore, the mismatches must be compensated in order to improve the performance of the acquisition system.

To calibrate the channel mismatches, numerous effective calibration techniques have been proposed. Some analogue calibration techniques [7] have been investigated to calibrate the delay of the sampling clock by sample-and-hold circuits or controlled delay lines. However, the performance of analogue techniques is typically restricted to the circuit components, which may also introduce additional thermal noise. The accuracy of analogue calibration methods is often limited in situations with high frequency signals. In contrast, digital calibration techniques calculate and compensate for mismatches in the digital domain, which can effectively overcome the drawback of analogue calibration techniques.

Therefore, researchers have become increasingly interested in digital calibration techniques, and most studies are focused on gain and time skew mismatches. In general, digital calibration methods fall into two categories: foreground techniques and background techniques. The foreground methods, such as sine fitting [8], frequency spectrum analysis [9], and the perfect reconstruction algorithm [10, 11], typically require a prior known signal to estimate the channel mismatches. In addition to these classical methods, some novel approaches are also presented [12, 13]. A *non-return-to-zero* (NRZ) signal is used as the reference signal in [12], and the mismatches are calibrated by the genetic algorithm. Furthermore, [13] provides a mismatch estimation method using the particle swarm optimization algorithm. The drawback of foreground methods is that the entire process is accomplished prior to signal acquisition, and the calibration structure does not change with the input signal. As it comes to background approaches, the calibration system can work in parallel with the acquisition system so that the calibration does not interrupt the operation of ADCs. The calibration algorithms only rely on the output of the acquisition system without requiring any input signal information.

Many background calibration techniques are based on an “estimation-compensation” strategy, and the design of filters is an important aspect of the calibration algorithm. Conventionally, it is customary to employ in the compensation block a bank of filters [14–16]. For example, a bank of compensation filters is employed in [16] based on the *least squares* (LS) method, which is essentially an inversion of the channel frequency response function. The filter coefficients should be calculated in advance, and if the system has a large number of channels, the whole calibration structure will be complicated. The first-order Taylor series approximation model is extensively used to correct the time skew mismatch by reconstructing the error signal from the product of the time skew value and the first-order differential signal [17–20]. Due to the calculation of the differential signal, derivative *finite impulse response* (FIR) filters are required. In practice, the order of the digital differentiator as well as the group delay may affect the final calibration performance. Furthermore, to ensure that the calibration strategies are suitable for the case of higher *Nyquist band* (NB) sampling, additional Hilbert filters are utilized in [16, 18, 20], thereby increasing the complexity of the calibration system. A novel calibration structure for gain and time skew mismatches is considered in [20, 21]. Even though the number of filters in the calibration process has decreased, digital differentiators are still required to calculate the first-order differential signals. Alternatively, a calibration scheme based on the Hilbert transform is presented in [22–25]. For example, in [22], the authors used the Hilbert transform to generate the basic functions of the error signal. However, the implementation of this method must rely on a Hilbert FIR filter, and both the real and imaginary parts of the signal are considered in the calculations. In scenarios with a large number of system channels, the computation of the iterative algorithm becomes complicated.

In this paper, a digital background calibration technique is proposed. First, the relationship between the input signal and the spurious signal caused by channel mismatches is analysed, and then the spurious signal can be represented using frequency-shifted signals that can be derived directly from the output of the TIADC. The Hadamard transform is utilized to generate frequency-shifted signals. Secondly, the mismatch coefficients are calculated by an adaptive iterative algorithm, and the spurious signal can be derived from the generated frequency-shifted signal and the coefficients. In this way, a bank of FIR filters commonly used in conventional methods can be omitted, which can simplify the calibration circuits. Moreover, our proposed method requires neither the digital differentiator in [21] nor the Hilbert filter in [22]. In general, the following are the main benefits of this work: (1) The proposed calibration structure eliminates the need for a filter, thereby simplifying the calibration circuit and decreasing its area and power consumption. (2) Instead of considering both the real and imaginary components of the signal, our method only needs to compute the real signal since the modulation sequence used contains only 1 and  $-1$ . This indicates that our proposed calibration scheme does not require a complex signal processing module.

The rest of this paper is organized as follows. Section 2 describes the TIADC acquisition system, as well as the spurious signal model. The proposed calibration approach using the modulated signals is proposed in Section 3. Section 4 reports some simulations and the experimental result of the proposed method. Finally, the conclusions are summarized in Section 5.

## 2. The model of a TIADC system

A typical TIADC system is made up of  $M$  sub-ADCs with the same resolution and sampling rate. The sub-ADC sampling rate in each channel is  $f_s/M$ , and the sampling clock phase of adjacent sub-ADC is different by  $2\pi/M$ . Then the total output is obtained by multiplexing the sub-ADC outputs. In this way, the sampling rate of the TIADC can be increased  $M$  times, which means that the equivalent sampling rate of the TIADC is  $f_s$ . Now we investigate the channel mismatches that would seriously degrade the performance of TIADCs, including gain, time skew, and offset mismatches. Assuming that  $x(t)$  is a band limited signal, the  $m$ -th sub-ADC output can be written as

$$y_m[n] = (1 + g_m)x((nM + m)T_s + \delta_m) + o_m, \quad (1)$$

where  $T_s$  is the sampling period, and  $o_m$ ,  $g_m$ , and  $\delta_m$  represent offset mismatch, gain mismatch, and time skew mismatch, respectively. Figure 1 depicts the mismatch model of a TIADC system. Note that the mismatches of the ADC are integrated into the channel frequency response and other errors are ignored, *i.e.*, all sub-ADCs are viewed as ideal in this model.

As for the offset mismatch, it is independent of the input signal, which can be readily compensated using the averaging method [26]. The sequence of one sub-ADC with the offset mismatch eliminated can be given as

$$\hat{y}_{m,o} = y_m[n] - \frac{1}{N} \sum_{n=1}^N y_m[n]. \quad (2)$$

According to (2), the offset mismatch could be calibrated rapidly by calculating the expected value of the sub-ADC output and then subtracting the corresponding value from the output sequence. Therefore, the proposed calibration technique provided in Section 3 will concentrate on the gain and time skew mismatches.

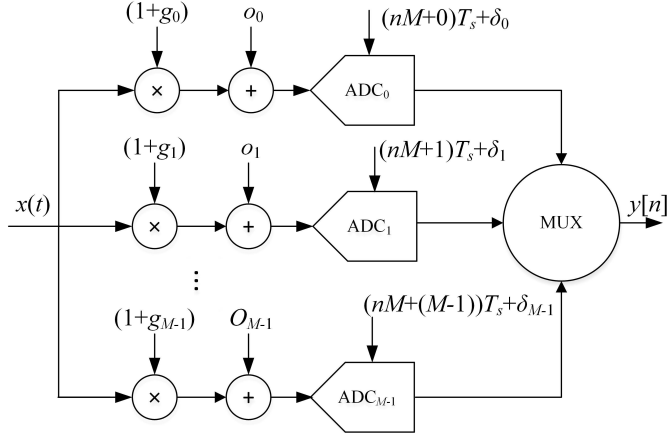


Fig. 1. Diagram of the channel mismatch model.

### 3. Proposed technique

#### 3.1. Spurious signals analysis

The output of a sub-ADC in the time domain has been introduced in Section 2. Generally, the frequency domain output of an  $M$ -channel TIADC can be represented as [27]

$$Y(j\omega) = \frac{1}{M} \sum_{k=0}^{M-1} \sum_{m=0}^{M-1} H_m \left( j \left( \omega - \frac{2\pi k}{M} \right) \right) X \left( j \left( \omega - \frac{2\pi k}{M} \right) \right) e^{-jkm \frac{2\pi}{M}}, \quad (3)$$

where  $X(j\omega)$  and  $Y(j\omega)$  are the input spectrum and output spectrum, respectively.  $H_m(j\omega)$  is the channel frequency response, which can be written as [22]

$$H_m(j\omega) = (1 + g_m) e^{-j\omega\delta_m}. \quad (4)$$

The frequency response of each channel in (3) can be combined, and (3) can be reformulated as

$$Y(j\omega) = \sum_{k=0}^{M-1} \alpha_k \left( j \left( \omega - \frac{2\pi k}{M} \right) \right) X \left( j \left( \omega - \frac{2\pi k}{M} \right) \right), \quad (5)$$

with

$$\alpha_k(j\omega) = \frac{1}{M} \sum_{m=0}^{M-1} H_m(j\omega) e^{-jkm \frac{2\pi}{M}}. \quad (6)$$

When  $k = 0$ , (5) represents the desirable signal spectrum. When  $k \neq 0$ , it is the spurious signal due to the channel mismatches, which should be eliminated. Therefore, (5) can also be written as desirable and spurious signals

$$Y(j\omega) = X_{\text{ideal}}(j\omega) + E(j\omega), \quad (7)$$

where

$$X_{\text{ideal}}(j\omega) = \alpha_0(j\omega) X(j\omega), \quad (8)$$

and

$$E(j\omega) = \sum_{k=1}^{M-1} \alpha_k \left( j \left( \omega - \frac{2\pi k}{M} \right) \right) X \left( j \left( \omega - \frac{2\pi k}{M} \right) \right). \quad (9)$$

The relationship between the spurious signals due to gain and time skew mismatches and the input signal has been established. Specifically, a two-channel system example is depicted in Fig. 2. One conclusion derived from (5)–(9) is that spurious signals caused by gain and time skew mismatches are obtained by frequency shifting and amplitude modulation of the input signal. In other words, the key to reconstructing the spurious signals is to attain a frequency-shifted version of the ideal signal. These frequency-shifted signals can be regarded as the basic function of the spurious signals. In this discrete model, the basic functions are labelled in the graph and they are generated by the modulation module. In summary, the reconstruction of the spurious signals can be divided into two steps: 1) The first is to shift the ideal signal spectrum to the frequency location where the spurious signals emerge to construct the basic functions. 2) The spurious signals that should be eliminated can be computed by the generated basic functions with a suitable set of mismatch coefficients. According to [22], the  $M$ -channel TIADC output can be amended as

$$Y(j\omega) = X_{\text{ideal}}(j\omega) + \sum_{k=1}^{M-1} \omega_k E_{f,k}(j\omega), \quad (10)$$

where  $\omega_k$  is the mismatch coefficient and  $E_{f,k}(j\omega)$  denotes the frequency-shifted form of the ideal signal, which can also be called the basis function of the spurious signal. It can be expressed as

$$E_{f,k}(j\omega) = X_{\text{ideal}} \left( j \left( \omega - \frac{2\pi k}{M} \right) \right). \quad (11)$$

### 3.2. Frequency-shifted signals generation

In this subsection, we will investigate the modulation module illustrated in Fig. 2 to generate the frequency-shifted signals required for the calibration technique. In [22], a scheme of basic function generation based on the Hilbert transform is proposed. The Hilbert filter is therefore an essential component of the calibration structure. Due to the utilization of exponential signal modulation after the Hilbert transform, the calculation takes into account both real and imaginary signals. In this paper, the Hadamard transform is used to implement the modulation module. Because the modulation sequence used contains only 1 and  $-1$ , our signal processing method only needs to consider the real signal and does not require additional filters. The method using the Hadamard transform is first presented in [21] to generate the pseudo aliasing signal.

Considering a four-channel TIADC system, a fourth-order Hadamard matrix is

$$\mathbf{F} = \begin{bmatrix} 1 & 1 & 1 & 1 \\ 1 & -1 & 1 & -1 \\ 1 & 1 & -1 & -1 \\ 1 & -1 & -1 & 1 \end{bmatrix}. \quad (12)$$

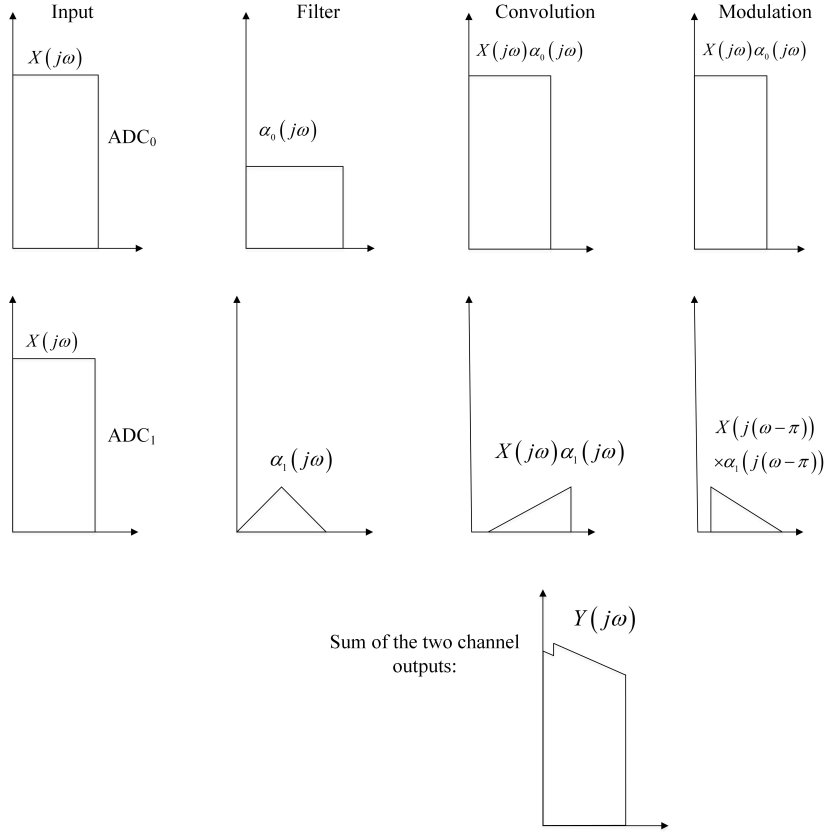


Fig. 2. Example of a two-channel system output.

The four rows of the Hadamard matrix shown in (12) can be used as four modulation sequences to modulate the ideal signal [21],

$$\mathbf{F} \cdot X_{\text{ideal}}(j\omega) = \begin{bmatrix} X_{\text{ideal}}(j\omega) \\ X_{\text{ideal}}(j(\omega - \pi/2)) \\ X_{\text{ideal}}(j(\omega - \pi)) \\ X_{\text{ideal}}(j(\omega - 3\pi/2)) \end{bmatrix}. \quad (13)$$

For the four sets of signals obtained in (13), the first row is the desired signal, while the remaining three rows are the frequency-shifted signals, *i.e.*, the basic functions, which can be used to represent the spurious signals. This processing is also shown in Fig. 3, where  $T_1$  to  $T_3$  represent the modulation sequences from the last three rows of the fourth-order Hadamard matrix. It should be noted that one prerequisite for employing this modulation method is that the number of channels of the acquisition system is specific, *e.g.*, 2, 4, 8, 16, *etc.* In other words, a Hadamard matrix must exist to correspond with the number of channels. In practice, the number of channels in most commercial TIADC systems is typically 2, 4, 8, *etc.*, which are powers of 2. Consequently, a corresponding Hadamard matrix is always available. As a result, the limitation of Hadamard transform modulation can be tolerated.

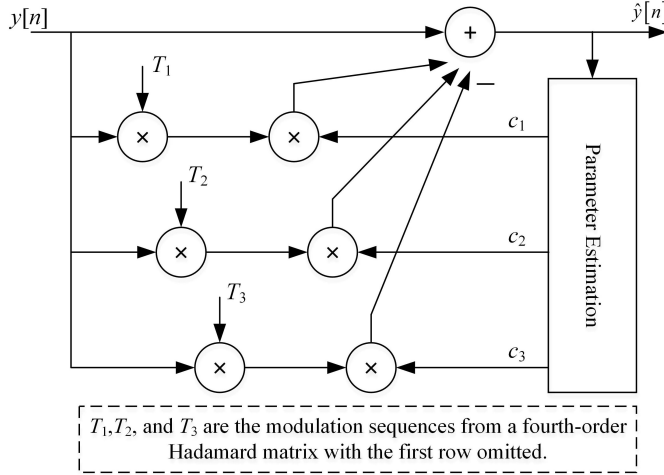


Fig. 3. Calibration structure of a four-channel TIADC.

### 3.3. Calibration algorithm

The frequency-shifted version of the desired signal and the spurious signals share identical frequency components following the Hadamard transform. As a result, the output of the acquisition system can be expressed by the frequency-shifted signals

$$y[n] = x_{\text{ideal}}[n] + \sum_{k=1}^{M-1} c_k x_{F,k}[n], \quad (14)$$

where  $c_k$  denotes the mismatch coefficient, and  $x_{F,k}[n]$  is the frequency-shifted signal generated by the Hadamard transform. Note that the ideal signal is known in (14). However, only the output signal of the system is usually available instead of the ideal signal. Therefore, as with most background calibration algorithms [17–22], we use the output signal  $y[n]$  instead of  $x[n]$  in our calculation.

A block diagram of the calibration structure used in a four-channel TIADC system is shown in Fig. 3.  $T_1$  to  $T_3$  are the modulation sequences used to modulate the output signal from a fourth-order Hadamard matrix. Note that at this time, the channel offset mismatch has been eliminated in advance. Since the frequency-shifted signals produced by the Hadamard transform have the same frequency components as the spurious signals, the error signals of the system can be reconstructed from the frequency-shifted signals weighted by a set of suitable coefficients. The “Parameter Estimation” module depicted in Fig. 3 is utilized to estimate the coefficient  $c_k$ . Once the coefficients are obtained, the mismatch error due to the gain and time skew mismatches can be computed and removed from the output to complete the calibration. The calibrated signal is expressed as

$$\hat{y}[n] = y[n] - \sum_{k=1}^{M-1} \hat{c}_k y_{F,k}[n], \quad (15)$$

where  $\hat{c}_k$  denotes the estimated value of the coefficient  $c_k$ . The entire calibration process is accomplished in the time domain without any filters or other complex signal processing. To complete the computation of the spurious signals, it is also necessary to acquire the weight coefficients for each frequency-shifted signal.

### 3.4. Coefficients estimation

In this subsection, the “Parameter Estimation” module in Fig. 3 is described. Fig. 4 shows the estimation block in a four-channel TIADC. A method based on the *least mean squares* (LMS) is proposed to estimate the coefficients adaptively. Additionally, the Hadamard transform is also applied to the calibration signal in the estimation module and the generated frequency-shifted signals are used as the input of the LMS block to estimate the mismatch coefficients. The iterative process of the algorithm is expressed by calculating the correlation between the calibration signal and the frequency-shifted signal, which is similar to the method described in [21, 22]. The iteration equation is

$$\hat{c}_k[n+1] = \hat{c}_k[n] + \mu (\hat{y}[n] \hat{y}_{F,k}[n]), \quad (16)$$

where  $\hat{y}_{F,k}[n]$  denotes the frequency-shifted form of the calibrated signal  $\hat{y}[n]$ , and  $\mu$  is the adaptation step size for  $\hat{c}_k$ . With the elimination of spurious signals, the feedback makes the value of the correlation function converge to 0. Once the estimated coefficients have been acquired, the calibrated signal can be obtained according to (15).

Additionally, one limitation of this method, as well as other similar methods [20, 21], should be mentioned. The frequency of a single-tone input to the acquisition system should avoid  $k\pi/M$ . This is because the frequency-shifted signal generated at this frequency point overlaps the input signal. The conventional method to resolve this limitation is to use a notch filter.

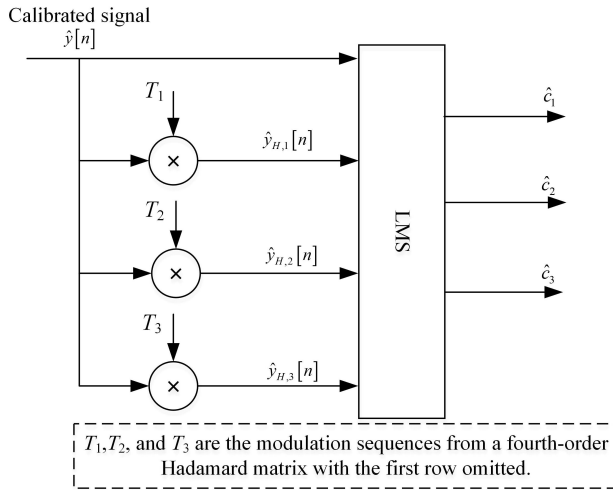


Fig. 4. The diagram of the parameter estimation module of a four-channel TIADC.

## 4. Experimental results

### 4.1. Simulation on a four-channel TIADC system

The calibration simulation of a 12.5 GSPS four-channel TIADC acquisition system is presented here. Gain, time skew, and offset mismatches are taken into account in the simulations, ignoring the effect of other errors such as quantization or jitter noise. First, a single-tone signal is considered, and the input frequency of the signal is  $f_{in} = 0.2fs$ . The coefficients of the channel mismatches are set as:  $o_m = [0, 0.04, -0.03, -0.05]$ ,  $g_m = [0, 0.06, -0.05, -0.07]$ , and  $\delta_m = [0, 0.12, -0.08, 0.14] \cdot T_s$ .

The magnitude of the input signal is 1 and  $T_s$  is the sampling period of the TIADC. The first channel is considered the reference channel, and we assume it is free of mismatch errors. The number of samples is 40K, and the iteration step is  $2^{-12}$ . Based on the simulation results, we find that the coefficients usually obtained at an adaption step of less than  $2^{-10}$  are consistent with our expectations. We use the *spurious free dynamic range* (SFDR) as a metric to measure the performance of the calibration method. In the spectrogram, SFDR can be expressed as the difference between the signal spectrum and the maximum non-signal spectrum. The result is shown in Fig. 5, where Fig. 5a is the uncalibrated signal and Fig. 5b shows the signal spectrum of the calibrated signal. The SFDR was increased from 26.28 dB to 76.07 dB. It shows that the proposed method can calibrate the channel mismatches accurately. In addition, the convergence of the LMS algorithm is demonstrated in Fig. 6. With the adaptive iterative algorithm, the final estimated coefficients are  $c = [0.015, -0.005, 0.0131]$ . Notice that the estimated coefficients converge when the number of samples is greater than 20K.

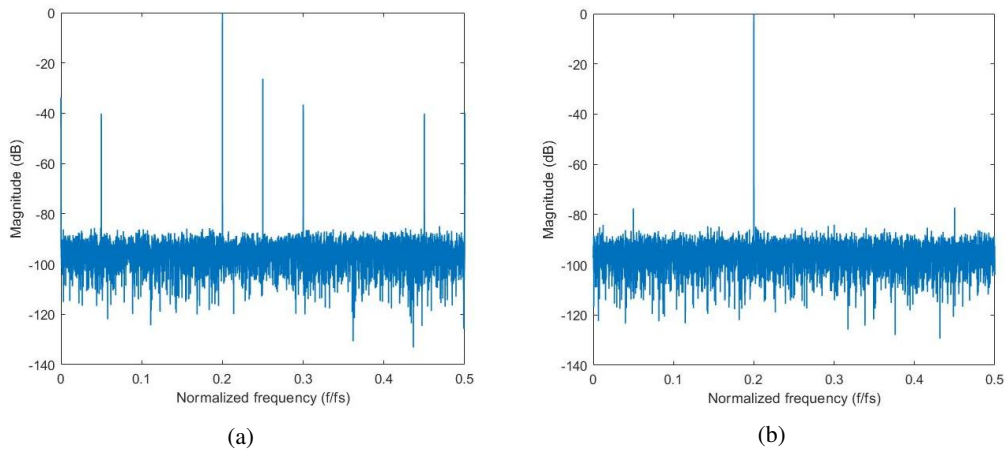


Fig. 5. Calibration performance of a four-channel TIADC (single-tone signal), a) is the uncalibrated signal spectrum, and b) is the spectrum of the calibrated signal.

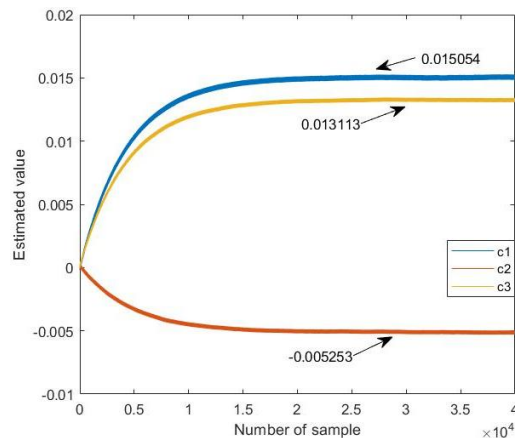


Fig. 6. Convergence curves of coefficients.

We also used a multi-tone signal to evaluate the calibration performance. The parameters are set as in the previous simulation, and the calibration result is shown in Fig. 7. In this simulation, the SFDR was increased from 26.35 dB to 70.63 dB. It demonstrated that the proposed calibration method gives an exceptional performance for single and multi-tone signals. In order to explore the effect of input signal frequency on the calibration method, a multi-tone signal containing different input frequencies was used to evaluate the performance of the calibration method. The frequency range of the input signal was 0 to  $f_s/2$ . For simplicity, the offset error was not considered in this simulation. The result is shown in Table 1. For the different input frequencies, the calibration algorithm can improve the SFDR by about 40 dB, which proves that the calibration algorithm is effective for the whole signal band.

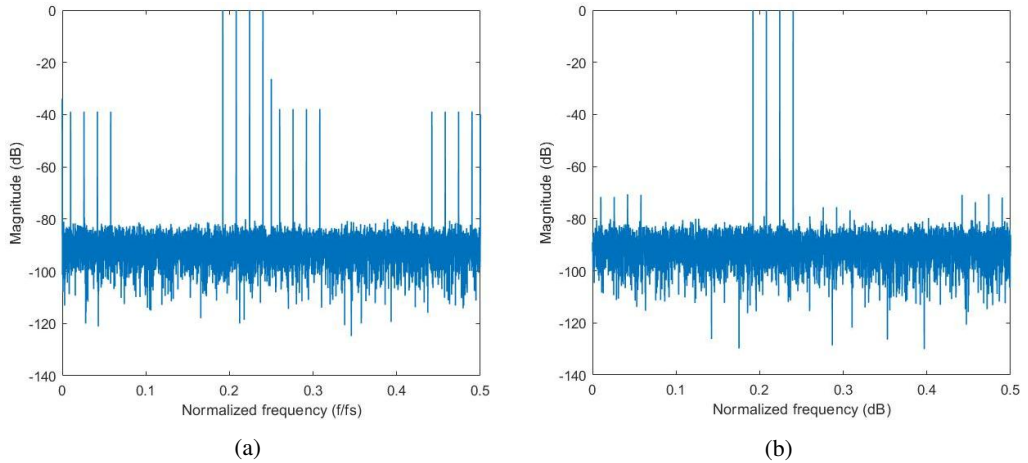


Fig. 7. Calibration performance of the four-channel TIADC (multi-tone signal), a) is the uncalibrated signal spectrum, and b) is the spectrum of the calibrated signal.

Table 1. Calibration performance of a multi-tone signal containing different input frequencies.

Input frequency	Maximum mismatch energy (uncalibrated)	Maximum mismatch energy (calibrated)
$0.1f_s$	-38.8 dB	-75.1 dB
$0.2f_s$	-36.5 dB	-76.0 dB
$0.3f_s$	-35.4 dB	-77.3 dB
$0.4f_s$	-34.2 dB	-77.5 dB
$0.45f_s$	-33.5 dB	-78.2 dB

#### 4.2. Comparison with other methods

A brief comparison between the proposed background calibration technique and the previous methods is shown in Table 2. The methods proposed in [17] and [18] only consider the time skew mismatch. For high-frequency input signals, the calibration performance of the method described

in [21] is decreased, whereas the method described in [21] must use a Hilbert filter to ensure the calibration performance. For example, the theoretical analysis of the method in [20] is identical to that in [21], except that a Hilbert filter is used in [20] to ensure the performance of the calibration algorithm at high-frequency inputs, which improves the SFDR by about 70 dB. However, the use of derivative filters and Hilbert filters is required in its calibration structure. The technique proposed in this paper is conceptually like the technique in [21], but it does not require any filter and has an advantage in convergence speed.

Table 2. Comparison with other methods.

Features	[17]	[18]	[21]	[22]	This work
Background calibration	Yes	Yes	Yes	Yes	Yes
Mismatch type	Time skew	Time skew	Gain Time skew	Gain Time skew Offset	Gain Time skew Offset
Number of channels	4	4	2	4	4
Input signal frequency	Multi-tone	$0.05f_s$ , $0.18f_s$ $0.29f_s$ , $0.405f_s$	$0.05f_s$ , $0.18f_s$ $0.29f_s$ , $0.405f_s$	$0.2f_s$	$0.2f_s$
Filters	Derivative filter	Derivative filter Hilbert filter	Derivative filter	Hilbert filter	No need
Convergence rate	110K	10K	30K	40K	20K
SFDR improvement	38 dB	40 dB	34 dB	44 dB	50 dB

#### 4.3. Experimental results

In this subsection, the technique proposed in this paper is also validated on a hardware platform. The method is tested on a 12.5 GSPS four-channel TIADC system. Specifically, the whole acquisition system mainly consists of a *radio frequency* (RF) signal generator, a four-channel TIADC system, and an *Industrial Control Computer* (ICC), as shown in Fig. 8a. The RF generator (SMA 100B from R&S) is utilized to generate the input signals which are fed into the TIADC system after passing through a conditioning channel and a power-splitting network. The purpose of the power-splitting network is to split the signal into multiple channels for parallel sampling. Two dual-core ADCs (ADC08DJ3200) are utilized to acquire the signals. Each ADC contains two sub-core ADCs, and it can be considered a four-channel TIADC system. A field-programmable gate array (FPGA, XCKU060-2FFVA1156) is used first to store the acquired samples, and then the samples are transmitted through the *peripheral component interconnect express* (PCIE) bus to the ICC. Fig. 8b depicts the prototype of the TIADC acquisition system.

The samples acquired by the above acquisition system were used to validate the calibration method proposed in this paper. In this experiment, a 4 GHz single-tone signal is used as the input signal to evaluate the calibration technique. The result is shown in Fig. 9. It can be noted that the spurious signals decreased after the calibration. The SFDR was increased from 22 dB to 47 dB, which validates the effectiveness of the proposed calibration technique. Since the test signals used also include some harmonics and other noises, and the calibration algorithm is ineffective against these errors, the result of the SFDR improvement is not as good as that of the simulation result.

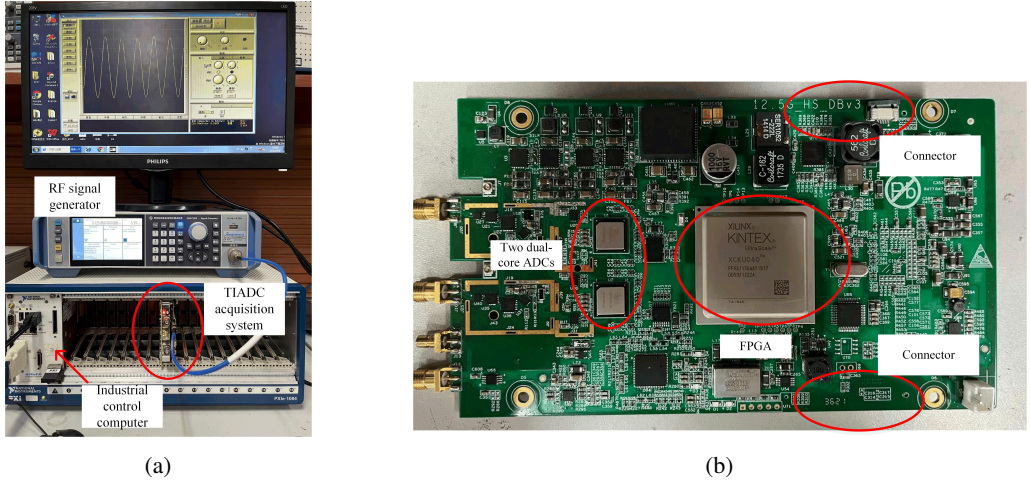


Fig. 8. 12.5 GSPS four-channel TIADC system hardware platform, a) is the whole acquisition system, and b) is the prototype of the acquisition system.

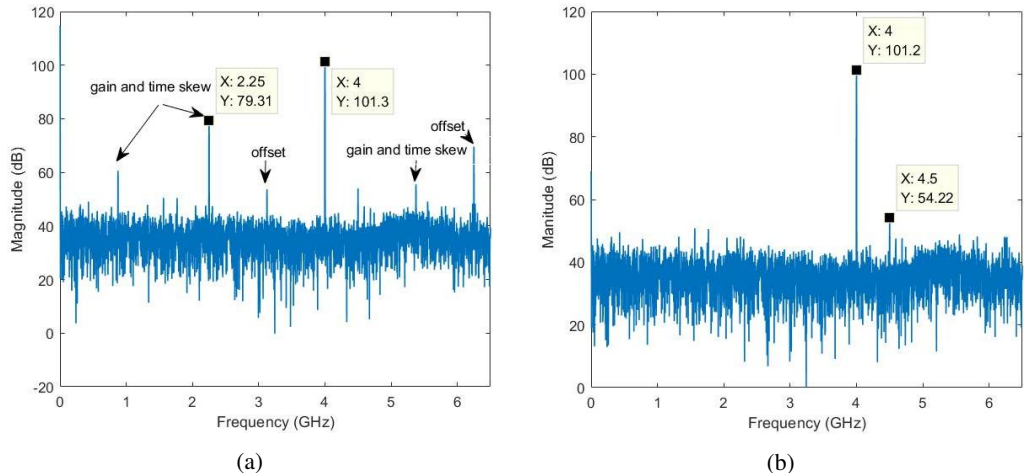


Fig. 9. 4 GHz single-tone signal calibration performance, a) is the uncalibrated signal spectrum, and b) is the spectrum of the calibrated signal.

## 5. Conclusions

In this paper, we focused on the channel mismatch calibration of TIADCs. In our work, the frequency-shifted signals are first generated using the Hadamard matrix modulation and then the coefficients are iteratively computed by the LMS algorithm, from which the spurious signals due to the channel mismatches are calculated. Compared with the previous methods, the proposed technique does not require any filters and other complicated signal processing. Furthermore, our method can offer an advantage in terms of convergence speed. Several simulations and experiments were

performed to evaluate the proposed technique. We have tested the proposed calibration technique in the four-channel TIADC acquisition systems and the results show that this method achieves a considerable improvement in SFDR. It is suitable for different TIADC systems as long as there exists a Hadamard matrix corresponding to the number of channels. The proposed method does not require any filters and therefore can significantly reduce the area and complexity of the calibration circuit.

### Acknowledgements

This work was supported in part by the Natural Science Foundation of the Sichuan Province under Grant 24NSFSC1520, and the Fundamental Research Funds for the Central Universities under Grant ZYGX2020ZB001.

### References

- [1] Zheng, Y., Zhao, Y., Zhou, N., Wang, H., & Jiang, D. (2021). A short review of some analog-to-digital converters resolution enhancement methods. *Measurement*, 180, 109554. <https://doi.org/10.1016/j.measurement.2021.109554>
- [2] Song, J., An, J., Bu, X., Gao, X., & Hu, Y. H. (2021). Time- and Frequency-Interleaving: Distinctions and Connections. *IEEE Transactions on Signal Processing*, 69, 2555–2568. <https://doi.org/10.1109/TSP.2021.3074013>
- [3] Black, W. C., & Hodges, D. A. (1980). Time interleaved converter arrays. *IEEE Journal of Solid-State Circuits*, 15(6), 1022–1029. <https://doi.org/10.1109/JSSC.1980.1051512>
- [4] Buchwald, A. (2016). High-speed time interleaved ADCs. *IEEE Circuits and Systems Magazine*, 54(4), 71–77. <https://doi.org/10.1109/MCOM.2016.7452269>
- [5] Kurosawa, N., Kobayashi, H., Maruyama, K., Sugawara, H., & Kobayashi, K. (2001). Explicit analysis of channel mismatch effects in time-interleaved ADC systems. *IEEE Transactions on Circuits and Systems I: Fundamental Theory and Applications*, 48(3), 261–271. <https://doi.org/10.1109/81.915383>
- [6] Vogel, C. (2005). The impact of combined channel mismatch effects in time-interleaved ADCs. *IEEE Transactions on Instrumentation and Measurement*, 54(1), 415–427. <https://doi.org/10.1109/TIM.2004.834046>
- [7] Bonavolontà, F., d'Arco, M., De Benedetto, E., Dallet, D., & Tedesco, A. (2021). A Review of Streamline Calibration Approaches for Digital Storage Oscilloscopes with Time-Interleaved Channels. *IEEE Instrumentation & Measurement Magazine*, 24(4), 11–17. <https://doi.org/10.1109/MIM.2021.9448259>
- [8] Li, J., Pan, J., & Zhang, Y. (2019). Automatic calibration method of channel mismatches for wideband TI-ADC system. *Electronics*, 8(1), 1–13. <https://doi.org/10.3390/electronics8010056>
- [9] Yang, K., Pan, Z., Ye, P., Shi, J., Zhao, Y., & Meng, J. (2021). A fast Fourier transform based method to estimate frequency response mismatches in time interleaved systems. *Review of Scientific Instruments*, 92(5), 054709. <https://doi.org/10.1063/5.0045246>
- [10] Zhao, L., Jiang, Z., Dong, R., Cao, Z., Gao, X., Cheng, B., Hu, J., Liu, S., & An, Q. (2018). An 8-Gs/s 12-bit TIADC system with real-time broadband mismatch error correction. *IEEE Transactions on Nuclear Science*, 65(12), 2892–2900. <https://doi.org/10.1109/TNS.2018.2878875>
- [11] Peng, X., Zhang, Y., Wang, W., & Yang, S. (2021). Broadband mismatch calibration for time-interleaved ADC based on linear frequency modulated signal. *IEEE Transactions on Circuits and Systems I: Regular Papers*, 68(9), 3621–3630. <https://doi.org/10.1109/TCSI.2021.3086065>

- [12] Tavares, Y. A., & Lee, M. (2021). A foreground calibration for M-channel time-interleaved analog-to-digital converters based on genetic algorithm. *IEEE Transactions on Circuits and Systems I: Regular Papers*, 68(4), 1444–1457. <https://doi.org/10.1109/TCSI.2021.3051612>
- [13] Zheng, Y., Zhou, N., Zhao, Y., & Sun, S. (2022). Time-interleaved system mismatch estimation based on correlation function and particle swarm optimization algorithm. *Review of Scientific Instruments*, 93(10), 104702. <https://doi.org/10.1063/5.0103225>
- [14] Tsai, T. H., Hurst, P. J., & Lewis, S. H. (2008). Correction of mismatches in a time-interleaved analog-to-digital converter in an adaptively equalized digital communication receiver. *IEEE Transactions on Circuits and Systems I: Regular Papers*, 56(2), 307–319. <https://doi.org/10.1109/TCSI.2008.2002114>
- [15] Han, C., Liu, S., Zhang, Y., Feng, L., Liang, H., & Zhu, Z. (2023). An all-digital background calibration technique for M-channel downsampling time-interleaved ADCs based on interpolation. *IEEE Transactions on Circuits and Systems II: Express Briefs*, 56(2), 307–319. <https://doi.org/10.1109/TCSII.2022.3233413>
- [16] Hu, M., & Yi, P. (2022). Digital calibration for gain, time skew, and bandwidth mismatch in under-sampling time-interleaved system. *Applied Sciences*, 12(21), 11029. <https://doi.org/10.3390/app122111029>
- [17] Liu, S., Zhao, L., & Li, S. (2022). A novel all-digital calibration method for timing mismatch in time-interleaved ADC based on modulation matrix. *IEEE Transactions on Circuits and Systems I: Regular Papers*, 69(7), 2955–2967. <https://doi.org/10.1109/TCSI.2022.3163431>
- [18] Le Duc, H., Nguyen, D. M., Jabbour, C., Graba, T., Desgreys, P., & Jamin, O. (2015). All-digital calibration of timing skews for TIADCs using the polyphase decomposition. *IEEE Transactions on Circuits and Systems II: Express Briefs*, 63(1), 99–103. <https://doi.org/10.1109/TCSII.2015.2483423>
- [19] Xiong, W., Zhang, Z., Lang, L., & Dong, Y. (2023). A novel fully digital feedforward background calibration technique for timing mismatch in M-channel time-interleaved ADCs. *Electronics*, 12, 1965. <https://doi.org/10.3390/electronics12091965>
- [20] Ta, V. T., Hoang, V. P., Pham, V. P., & Pham, C. K. (2020). An improved all-digital background calibration technique for channel mismatches in high speed time-interleaved analog-to-digital converters. *Electronics*, 9(1), 73. <https://doi.org/10.3390/electronics9010073>
- [21] Matsuno, J., Yamaji, T., Furuta, M., & Itakura, T. (2013). All-digital background calibration technique for time-interleaved ADC using pseudo aliasing signal. *IEEE Transactions on Circuits and Systems I: Regular Papers*, 60(5), 1113–1121. <https://doi.org/10.1109/TCSI.2013.2249176>
- [22] Qiu, Y., Liu, Y. J., Zhou, J., Zhang, G., Chen, D., & Du, N. (2018). All-digital blind background calibration technique for any channel time-interleaved ADC. *IEEE Transactions on Circuits and Systems I: Regular Papers*, 65(8), 2503–2514. <https://doi.org/10.1109/TCSI.2018.2794529>
- [23] Bonnetat, A., Hodé, J., Ferré, G., & Dallet, D. (2015). Correlation-based frequency-response mismatch compensation of quad-TIADC using real samples. *IEEE Transactions on Circuits and Systems II: Express Briefs*, 62(8), 746–750. <https://doi.org/10.1109/TCSII.2015.2433472>
- [24] Bonnetat, A., Hodé, J., Ferré, G., & Dallet, D. (2015). An adaptive all-digital blind compensation of dual-TIADC frequency response mismatch based on complex signal correlations. *IEEE Transactions on Circuits and Systems II: Express Briefs*, 62(9), 821–825. <https://doi.org/10.1109/TCSII.2015.2435611>
- [25] Sun, L., Lang, L., Zhong, W., Liu, H., & Dong, Y. (2023). A fast mismatch calibration method based on frequency domain orthogonal decomposition for time-interleaved analog-to-digital converters. *Electronics*, 12, 5042. <https://doi.org/10.3390/electronics12245042>

- [26] Guo, L., Tian, S., & Wang, Z. (2014). Estimation and correction of gain mismatch and timing error in time-interleaved ADCs based on DFT. *Metrology and Measurement Systems*, 21(3), 535–544. <https://doi.org/10.2478/mms-2014-0045>
- [27] Vogel, C., & Mendel, S. (2009). A flexible and scalable structure to compensate frequency response mismatches in time-interleaved ADCs. *IEEE Transactions on Circuits and Systems I: Regular Papers*, 56(11), 2463–2475. <https://doi.org/10.1109/TCSI.2009.2015595>



**Yanze Zheng** received his B.Sc. degree from Southwest Petroleum University, China, in 2017. He is currently working towards his Ph.D. degree at the University of Electronic Science and Technology of China. His current research interests include digital signal processing, instrumentation and measurement technology.



**Sitao Mei** received both his B.Sc. and M.Sc. degrees, in 2018 and 2021 from the University of Electronic Science and Technology of China. He is currently working towards his Ph.D. degree at the same university. His current research interests include digital signal processing, instrumentation and measurement technology.



**Sicheng Sun** received his M.Sc. degree from the University of Electronic Science and Technology of China, China, in 2013. He is currently working towards his Ph.D. degree at the same university. His current research interests include the phased array technique and SAT-COM array.



**Yijiu Zhao** received his B.Sc., M.Sc. and Ph.D. degrees in 2004, 2007 and 2012 from the University of Electronic Science and Technology of China. He is currently a professor at the same university. His current research interests include compressed sensing, signal processing, and analog signal sampling.